

Preparation of graphene-based active carbons from petroleum asphalt for high-performance supercapacitors without added conducting materials

WANG Bin^{1,4}, XIE PengYi¹, ZHANG Miao^{2*}, ZHANG HongTao^{3*} & CHEN YongSheng³¹ School of Physics and Materials Science, Guangzhou University, Guangzhou 510006, China;² School of Chemistry and Materials Science, Guangdong University of Education, Guangzhou 510303, China;³ The Centre of Nanoscale Science and Technology and Key Laboratory of Functional Polymer Materials, Institute of Polymer Chemistry, College of Chemistry, Nankai University, Tianjin 300071, China;⁴ Research Center for Advanced Information Materials (CAIM), Huangpu Research & Graduate School of Guangzhou University, Guangzhou 510555, China

Received June 23, 2022; accepted September 13, 2022; published online November 18, 2022

Graphene-based active carbons (G-ACs) with a high specific surface area and high conductivity are promising electrode materials for high-performance supercapacitors. Typically, however, syntheses of the G-ACs call for expensive raw materials and are cumbersome. Here, the G-ACs are obtained by direct chemical activation of petroleum asphalt. The highest specific surface area of the prepared G-ACs is 3505 m²/g and the corresponding conductivity is 32 S/m. Electrodes fabricated using the as-prepared G-ACs, i.e., without any conductive additives, demonstrate high specific capacitance and high rate performance. The specific capacitances of optimized G-ACs, as measured in a 1 mol/L TEABF₄/AN electrolyte and the neat ionic liquid EMIMBF₄, are 155 and 176 F/g at 1 A/g, providing the high energy density of 39.2 and 74.9 W h/kg, respectively. In addition, the G-ACs exhibited excellent rate capability with a negligible capacitance decay from 0.5 to 10 A/g in both 1 mol/L TEABF₄/AN and neat EMIMBF₄ electrolytes. Furthermore, the optimized G-AC has a high energy density (68.5 W h/kg) at a relatively high power density (8501 W/kg), indicating that it holds potential for application in green energy storage.

supercapacitor, asphalt, porous carbon, rate capability

Citation: Wang B, Xie P Y, Zhang M, et al. Preparation of graphene-based active carbons from petroleum asphalt for high-performance supercapacitors without added conducting materials. *Sci China Tech Sci*, 2022, 65: 2866–2873, <https://doi.org/10.1007/s11431-022-2207-x>

1 Introduction

Among various energy storage devices, carbon-based supercapacitors are receiving considerable attention due to their rapid power delivery and excellent cycling stability [1–4]. However, their low energy density related to the relatively low surface area of commercial active carbon electrodes used in them precludes a broader use of these devices in various types of electrical appliances [5,6]. Some progress has been

made toward optimization of the storage capability of activated carbon materials for high energy density supercapacitors [7–10]. It is therefore desirable to design and synthesize advanced carbon materials with high electrical conductivity, high specific surface area (SSA), and appropriate porosity [11].

Graphene-based active carbons (G-ACs), a type of porous carbon materials mainly consisting of graphene sheets in a few nanometers, have both high electrical conductivity of crystalline sp² carbon materials and high SSA of amorphous carbon materials. Therefore, G-ACs are considered

*Corresponding authors (email: zmiao@gdei.edu.cn; htzhang@nankai.edu.cn)

promising electrode materials for supercapacitors [12–16]. They are usually synthesized from relatively high-cost graphene oxide (GO) or GO/carbon precursor composites (with the GO content of around 1%–7%) [17–19]. However, synthetic strategies for this type of G-ACs are technically quite complex and include, e.g., hydrothermal and activation processes. Therefore, there is a call for devising more facile and feasible methods for the preparation of G-ACs with high SSA and high conductivity from inexpensive starting materials [20–23].

Petroleum asphalt is a byproduct of the distillation of crude oil. It is inexpensive and broadly available. It consists of a mixture of a number of chemicals, with polycyclic aromatic hydrocarbons (PAHs) being its major components. These PAHs can be thought of as graphene fragments with functional groups [24–26]. The following two extremes may occur as a result of high-temperature treatment of the PAHs. (1) They covalently bonded via functional groups at the edges, which results in three-dimensional graphene networks. It also is possible to obtain a conductive graphene-like material by splicing PAH fragments into large area graphene sheets. (2) If the PAHs are stacked not through the edges but through π - π stacking, a graphite-like structure is obtained [27]. As a result, the cost of starting materials required for graphene-based carbon electrode materials can be greatly reduced. On the other hand, a typical synthesis of G-ACs usually consists of two main steps, i.e., hydrothermal processing and activation. If the preparation process can be simplified into a single-step process, the energy consumption for the synthesis of graphene-based carbons will be greatly reduced as well.

Based on the above analysis, we tried to obtain G-ACs with high SSA and high electrical conductivity by direct chemical activation of petroleum asphalt. For G-ACs prepared by this method, the highest SSA was 3505 m²/g and the conductivity was 32 S/m. The best values for the specific capacitances of our G-ACs in 1 mol/L tetraethylammonium tetrafluoroborate in acetonitrile (TEABF₄/AN) and the neat ionic liquid 1-ethyl-3-methylimidazolium tetrafluoroborate (EMIMBF₄) were 155 and 176 F/g at 1 A/g, respectively. In addition, our G-ACs, which had no added conductive materials, exhibited excellent rate capability with a negligible capacitance decay, from 0.5 to 10 A/g, in the 1 mol/L TEABF₄/AN and neat EMIMBF₄ electrolytes. Furthermore, the optimized G-AC had a high energy density (68.5 W h/kg) at a relatively high power density (8501 W/kg), indicating its potential use in green energy applications.

2 Materials and methods

2.1 Materials synthesis

Elemental analysis, softening point and thermogravimetric

analysis of the petroleum asphalt were listed in Table S1 and Figure S1. Petroleum asphalt (3 g) and KOH were separately ground into powder and then mixed at different mass ratios. The asphalt/KOH mixtures in different proportions were placed in a horizontal tube furnace and heated to 400°C for 1 h at a rate of 5°C/min and then kept at 900°C for 1 h under high purity Ar. The product was allowed to cool to room temperature and then washed repeatedly with boiling 0.1 mol/L HCl and water until the pH value decreased to ~7. The final products were obtained after vacuum drying at 120°C for 24 h; they were denoted by G-AC_{*n*}, i.e., G-AC1, G-AC2, G-AC3, and G-AC4, where *n* is the mass ratio of KOH to petroleum asphalt.

2.2 Characterization

Scanning electron microscopy (SEM) studies were performed on a Nova Nano 230 instrument operated at 10 kV, and tunneling electron microscopy (TEM) was performed on a JEOL TEM-2100 instrument operated at a voltage of 200 kV. Powder X-ray diffraction (XRD) analysis using Cu K α radiation was carried out on a Rigaku D/Max-2500 diffractometer. Nitrogen adsorption-desorption analysis (at 77 K) was performed on a Micromeritics ASAP 2020 apparatus. The Brunauer-Emmett-Teller (BET) method was used to calculate the surface area (the range of relative pressure p/p_0 spanned 0.05 to 0.3), and the pore size distribution (PSD) was analyzed by a non-local density functional theory (NL-DFT) method. Raman spectra were acquired with a LabRAM HR Raman spectrometer using a 514.5 nm laser for spectral excitation. Lorentzian fitting was carried out to obtain the positions and widths of the D and G bands in the Raman spectra. According to the Raman spectra, the size of the graphene domains La (nm) can be estimated using the equation $La = (2.4 \times 10^{-10}) \lambda^4 (I_D/I_G)^{-1}$, where λ is the laser energy in nanometers, and I_D and I_G are the intensities of the D and G bands, respectively. Samples for conductivity measurements were prepared as follows: the G-ACs were mixed with 1 wt% polytetrafluoroethylene (PTFE, DuPont) and rolled into 100 μ m thick films, then cut into 3 cm \times 1 cm strips, and their resistance R was measured. Conductivity λ of the sample strips was calculated according to the formula:

$$\lambda = \frac{L}{RWd}, \quad (1)$$

where L is the length of a strip, W and d are its width and thickness, respectively.

2.3 Fabrication of supercapacitors and their electrochemical characterization

G-AC and PTFE were combined at a mass ratio of 9:1, thoroughly mixed, and then rolled into sheets with a thickness of ~100 μ m (mass loading ~3.1 mg/cm²). To fabricate

electrodes, the sheets were punched into discs with a diameter of 12 mm and the discs were hot pressed onto the aluminum foil with a conductive carbon layer. The prepared electrodes were assembled into symmetrical capacitors which were filled with commercially available electrolytes: 1 mol/L tetraethylammonium tetrafluoroborate in acetonitrile (TEABF₄/AN, BASF) and the neat ionic liquid 1-ethyl-3-methylimidazolium tetrafluoroborate (EMIMBF₄). These capacitors were used in electrochemical tests.

Charge and discharge measurements were carried out using a LAND CT2001A test system (Wuhan LAND Electronics. Ltd.). Cyclic voltammetry (CV) and electrochemical impedance spectroscopy (EIS) measurements were performed using an Autolab system (Metrohm). The CV measurements were performed in the potential ranges spanning 0 to either 2.7 or 3.5 V, with the scanning rate being 50, 100, or 200 mV/s. The EIS measurements were carried out in the frequency range of 0.01 Hz to 100 kHz at an AC amplitude of 10 mV.

Real capacitance C' and imaginary capacitance C'' were calculated from the following two equations:

$$C' = \frac{Z''}{2\pi f|Z|^2}, \quad (2)$$

$$C'' = \frac{Z'}{2\pi f|Z|^2}, \quad (3)$$

where Z' and Z'' are the real and the imaginary parts of impedance Z , and f is the frequency (Hz).

The energy density E (W h/kg) and the (average) power density P (W/kg) of the symmetric supercapacitors were calculated according to eqs. (4) and (5), respectively:

$$E = C_s V^2 / 8, \quad (4)$$

$$P = E / \Delta t, \quad (5)$$

where V and Δt are the voltage and discharge time, respectively.

3 Results and discussion

The preparation process of G-AC from petroleum asphalt is schematized in Figure 1. During the high temperature activation process, parts of petroleum asphalt were converted

into three-dimensional graphene networks via covalently bonding of PAH functional groups at the edges. And the other parts of petroleum asphalt were transformed into graphite-like materials through π - π stacking of PAH fragments [27]. At the same time, the resulting composite material interacts with potassium hydroxide to give porous graphene-based carbon materials [28–30].

Our G-ACs were denoted by G-AC n , where n is the mass ratio of KOH to petroleum asphalt. SEM images of G-AC n are shown in Figure S2. It can be observed that the activated sample has a rough surface with porous morphology. G-AC3 (Figure 1(a) and (b)) has a pore size of \sim 200 nm. The pores were likely to have formed as a result of both self-assembly and activation of PAHs in the asphalts during high-temperature treatment. High-resolution TEM images of G-AC3 (Figure 2(c) and (d)) show that this sample consists of disorder networks of nanometer-sized graphene sheets with defects and folds [17]. They also show that G-AC3 has hierarchical porous structures, indicating that it may exhibit good performance in supercapacitors.

The specific defect structure of, and stacking order in, G-ACs can be characterized by Raman spectroscopy and XRD. In the spectra in Figure 3(a), the peaks at \sim 1320 cm⁻¹ (D-band) are assigned to defective graphitic or disordered carbon structures. The peaks near 1580 cm⁻¹ (referred to as the G-band) are assigned to the E_{2g} phonon of sp² carbon atoms [26]. The average size L_a (the in-plane size) of graphene domains was roughly estimated from the integral intensity ratio I_D/I_G of the D to G bands in the Raman spectrum [17]. It is worth noting that L_a of G-AC3 was estimated to be 6.6 nm, a value close to that of G-AC materials prepared using relatively expensive GO composites as starting materials (\sim 6.6 nm), but much smaller than that for products derived from pure GO (11.9 nm) or commercial active carbon YP50 (10.7 nm) [17]. Figure 3(b) shows the XRD patterns of our G-AC1, G-AC2, G-AC3, and G-AC4 porous carbon materials. All of the samples exhibit an extremely weak and very broad (002) peak in the range of 15°–25°, which suggests a more disordered structure with almost no stacking graphene domains [31]. The diffraction peak at 26.5° is the peak of graphite-like substances (002), which is the product of partial graphitization of asphalt at high temperatures [32]. X-ray photoelectron spectroscopy analysis

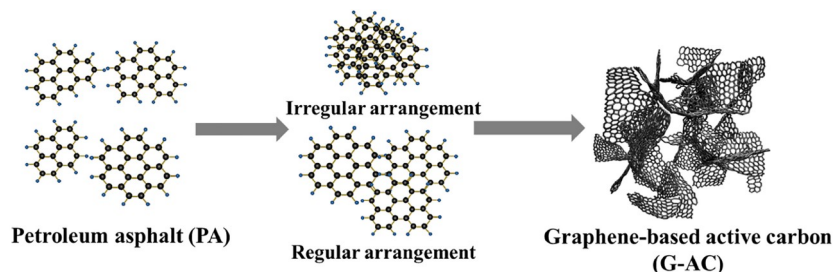


Figure 1 A diagram showing the carbonization/activation of G-AC materials.

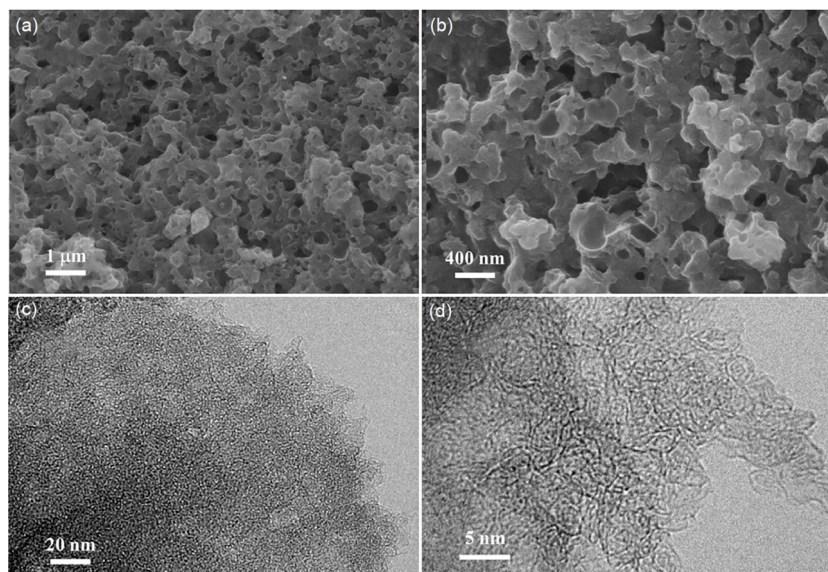


Figure 2 (a), (b) SEM images of G-AC3; (c) low- and (d) high-resolution TEM images of G-AC3.

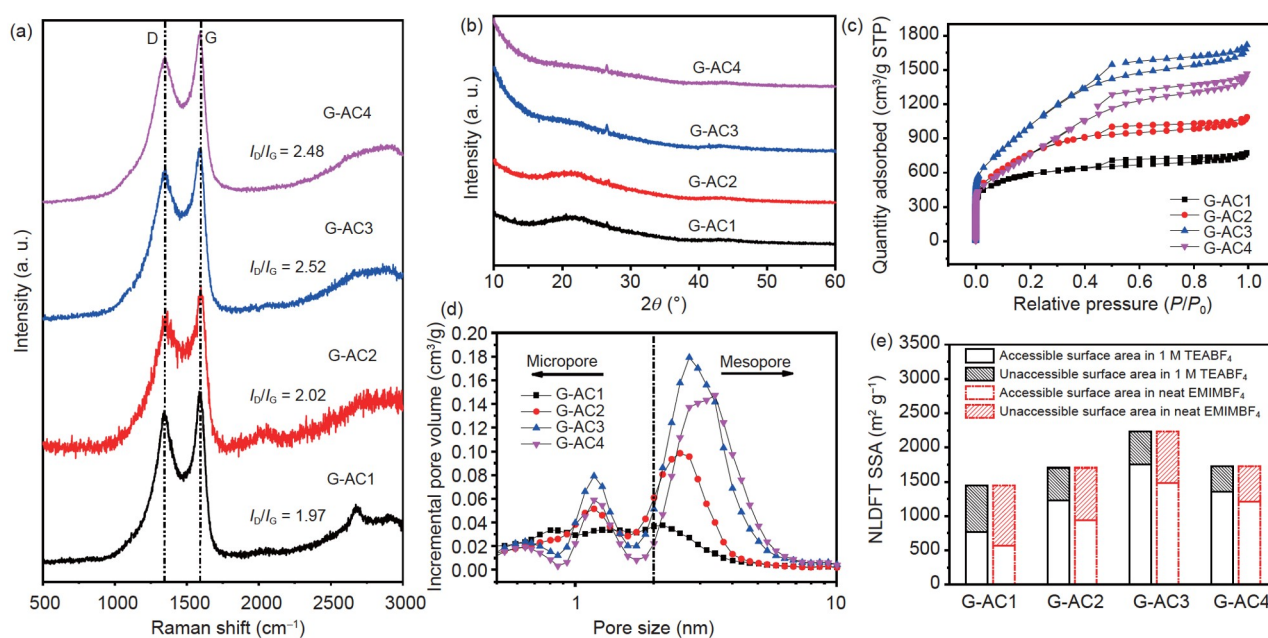


Figure 3 (Color online) (a) Raman and (b) XRD spectra of G-AC n . (c) N₂ adsorption-desorption isotherms of G-AC n ; (d) pore size distribution (PSD) calculated from the adsorption isotherms using a DFT method; (e) effective SSA of G-AC n when using TEABF₄ and EMIMBF₄ as electrolytes for supercapacitors.

further indicated the presence of a significant fraction of sp² carbons and a high C/O ratio (Figure S3).

The SSA and pore volume distribution of prepared materials were obtained from their N₂ adsorption/desorption isotherms. As can be observed in Figure 3(c), the experimental isotherms for our G-AC n samples can be classified as type IV isotherms, which are markedly different from those for YP50 (a type of commercial active carbon), which gives type I isotherms (Figure S4(a)). All our products have a large BET SSA, in excess of 2135 m²/g (Table 1). The highest

BET SSA was obtained for G-AC3, 3505 m²/g, a value much higher than that of YP50 (1676 m²/g).

Next, we analyzed the PSD of these materials. As shown in Figure 3(d) and Table 1, the majority of pores in our G-AC n materials are mesopores in the range of 2 to 7 nm; they also have micropores with a size <1 nm. The structure of this material is markedly different from the PSD of commercial YP50. Our G-AC n materials are mainly mesoporous, while the indicated commercial material is mainly microporous (Figure S4(b)). If the pore size of electrode material is too

Table 1 SSA, pore size, and conductivity of G-AC n and YP50^{a)}

Sample	BET SSA (m ² /g)	Pore volume (cm ³ /g)	Average pore size (nm)	Conductivity (S/m)
G-AC1	2135	0.30	2.73	15
G-AC2	2817	0.29	2.59	18
G-AC3	3505	1.21	2.39	32
G-AC4	2759	1.81	2.73	29
YP50				5
YP50*	1676	0.11	1.88	20

a) YP50* is the mixture of 90% YP50 and 10% conductive carbon black.

small, the relatively large electrolyte will not be able to access them [33]. The relatively high concentration of mesopores indicates that G-AC n has a larger effective SSA (E-SSA) available for the electrolyte ions. Figure 3(e) shows detailed E-SSAs for each of the G-AC samples, which were calculated for the positive ions TEA⁺ and EMIM⁺ with a size of ~0.61 and ~0.76 nm, respectively, which corresponds to using TEABF₄ and EMIMBF₄ as the electrolyte for supercapacitors [18], respectively. As a result, apart from the fact that our G-AC n has ultrahigh total SSA, their E-SSA for the considered electrolyte ions is much higher in comparison with that of the commercial active carbon.

In striving to fabricate advanced materials for supercapacitors, apart from the requirement of high SSA and proper PSD, the conductivity of the material must be considered. Our G-AC n materials have not only pore structures adequate for the transfer and adsorption of electrolyte ions, but they also show high electrical conductivity. In particular, G-AC3 has a conductivity of 32 S/m, which is higher than that of YP50 with 10% of added carbon black (20 S/m). It is therefore possible to fabricate a capacitor with excellent performance using G-AC3 without any conductive additives (such as carbon black).

In view of the high porosity and conductivity of the G-AC n materials, we used them without the addition of carbon black, a conductive additive, as the active electrode materials in supercapacitors. Figure 4 shows the electrochemical performance of supercapacitors fabricated using the G-AC n as the electrode material and 1 mol/L TEABF₄/AN as the electrolyte. All the devices displayed high specific capacitance (Figure 4(a)). Excellent results were obtained for a G-AC3-based supercapacitor, which had a specific capacitance of 155 F/g (much higher than that of YP50 with ~100 F/g at 1 A/g, Figure S5) and an energy density of 39.2 W h/kg at a current density of 1 A/g. Results of CV characterization of G-AC3 are presented in Figure 4(b). CV curves with a characteristic rectangular shape were recorded in the potential range of 0 to 2.7 V at a scan rate of 50, 100, 200, and 500 mV/s. The charge-discharge curves (Figure 4(c)) recorded at different current densities are quite symmetric and linear, which points to the effective formation of an electrochemical double layer (EDL). The specific capacitance of

G-AC3 calculated from the discharge curves was 154, 155, 159, 153, and 154 F/g at current densities of 0.5, 1, 2, 5, and 10 A/g, respectively. More importantly, G-AC3 exhibits excellent rate capability and columbic efficiency (Figure 4(d)). We attributed this superior rate capability to its high SSA, proper PSD, and high conductivity, which makes the interior surfaces of the electrode material more accessible to electrolyte ions and leads to an increase in the specific capacitance.

Figure 4(e) shows a Nyquist plot of G-AC3 recorded in the frequency range of 0.01 Hz to 100 kHz. The inset is an enlarged view of the high-frequency region. The Nyquist plot features an almost vertical line in the low-frequency region, which indicates a nearly ideal capacitive behavior. The frequency-dependent real and imaginary capacitances of G-AC3 are shown in Figure 4(f) and (g). The imaginary capacitance reaches its maximum value at a frequency of 0.95 Hz. The response time of the G-AC3 device was calculated to be only 1.05 s ($\tau_0=1/f_0$), which is shorter than for several other high-performance carbon-based capacitor materials reported previously; more specifically, for an alginate-based porous carbon and a frame-filling structural porous carbon the values were 2.4 and 5.34 s, respectively, in the same organic electrolyte [34,35]. Our G-AC3 material has a suitable pore structure and high electrical conductivity, which accounts for its high ion and electron transport rates, as indicated by its relatively small τ_0 and a fast frequency response. At a current density of 1 A/g the specific capacitance was maintained 92% of the initial value after 10000 cycles, indicating that the supercapacitor has good cycling stability (Figure 4(h)).

For a more detailed characterization of our samples as electrode materials for high-voltage supercapacitors, we used neat EMIMBF₄ as the electrolyte. As shown in Figure 5(a), G-AC n can display excellent specific capacitance in the neat EMIMBF₄ electrolyte due to its mesoporous structure and high SSA. In addition, the neat EMIMBF₄ electrolyte favors achieving a high operating voltage (3.5 V), which is much higher than in aqueous and organic electrolytes. The high specific capacitance along with the high operating voltage contributes to the high gravimetric energy density of our materials. The best result was observed for G-AC3,

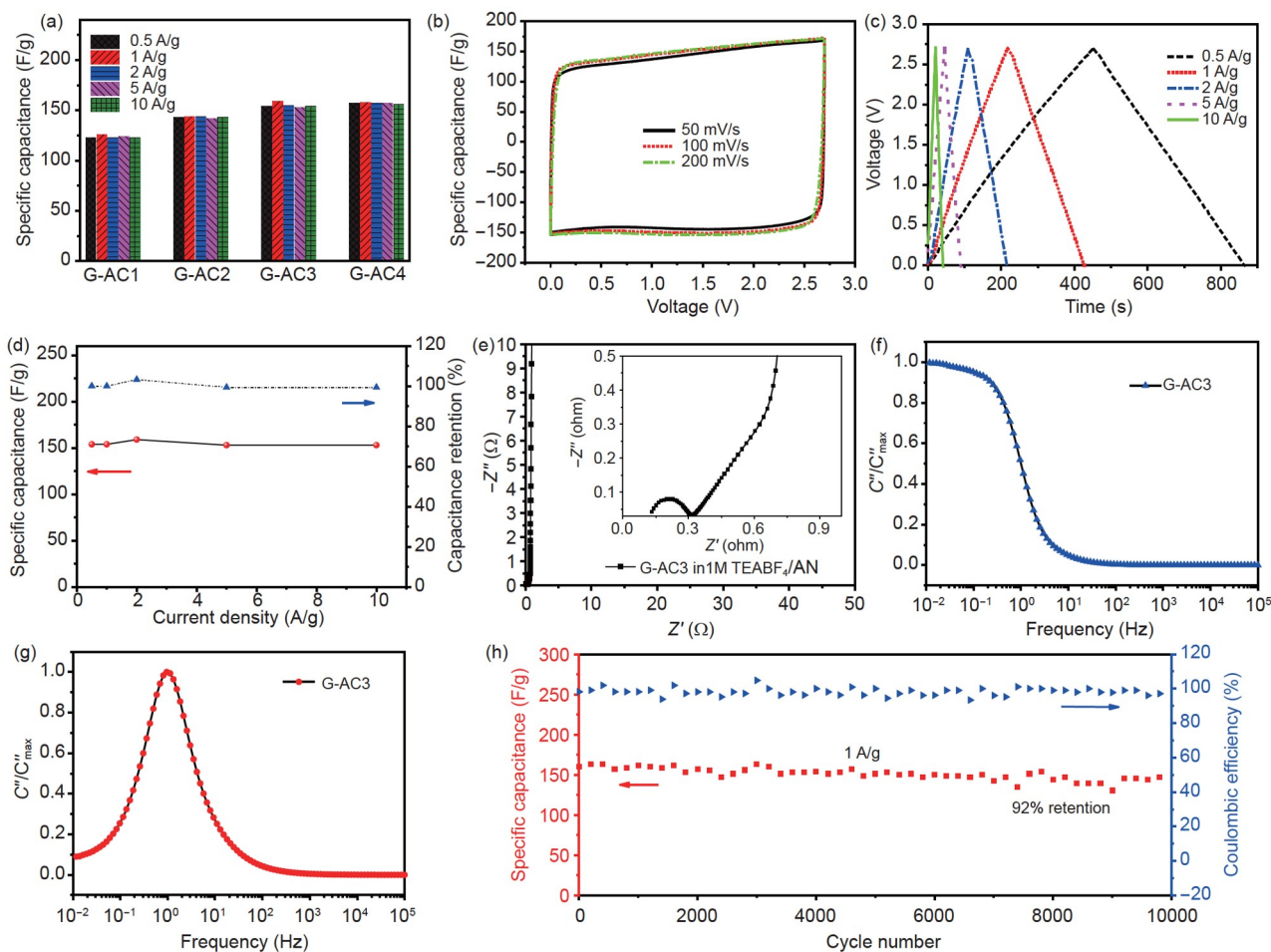


Figure 4 (Color online) Electrochemical characterization of the G-AC n samples in a 1 mol/L TEABF $_4$ /AN electrolyte. (a) Specific capacitances of the G-AC n at different current densities. (b) CV curves of G-AC3 at three different scan rates. (c) Charge/discharge curves of G-AC3 at different currents. (d) Rate performance using the G-AC3 samples as electrode materials. (e) Nyquist plots of the G-AC3-based supercapacitors. (f), (g) Frequency response curves of the real and imaginary capacitances of the G-AC3-based supercapacitors. (h) Cycling life of G-AC3 at a current density of 1 A/g.

which is 176 F/g at 1 A/g, giving an energy density of 74.9 W h/kg, its electrochemical performance in the neat EMIMBF $_4$ electrolyte is discussed in details below.

CV profiles of G-AC3 (Figure 5(b)) exhibit a characteristic EDL behavior at scan rates of 50, 100, and 200 mV/s in the neat EMIMBF $_4$ electrolyte. A slight distortion in the curve shape may be due to the larger viscosity of the neat ionic liquid [17,36]. All of the charge-discharge curves recorded at different currents (Figure 5(c)) are fairly symmetric and linear, a characteristic of the ideal double-layer capacitance behavior. The specific capacitance of the G-AC3 material obtained from the discharge curves is 176, 176, 172, 170, and 161 F/g at the current densities of 0.5, 1, 2, 5, and 10 A/g in the neat EMIMBF $_4$ electrolyte (Figure 5(d)). The excellent rate performance in the neat EMIMBF $_4$ electrolyte resulted from the three-dimensional structure and high conductivity of G-AC3 [37]. The Nyquist diagram in Figure 5(e) shows that the device has a low resistance due to rapid ion diffusion in channels G-AC3.

The cycling test for the G-AC3 showed ~85% capacity retention at a current density of 1 A/g after 9000 cycles, indicating good stability of the electrodes in the neat EMIMBF $_4$ electrolyte (Figure 5(f)). Finally, we calculated the energy density and power density of the supercapacitors with the EMIMBF $_4$ electrolyte from their electrochemical parameters. G-AC3 has an energy density of 74.9 W h/kg at a power output of 448 W/kg, retaining 68.5 W h/kg at 8501 W/kg.

4 Conclusions

Graphene-based active carbon materials were prepared from petroleum asphalt, a low-cost raw material, through a direct one-step process. The G-ACs were found to have a high specific surface area and high conductivity. The highest specific surface area of the prepared G-ACs was 3505 m 2 /g and the corresponding conductivity was 32 S/m. The specific

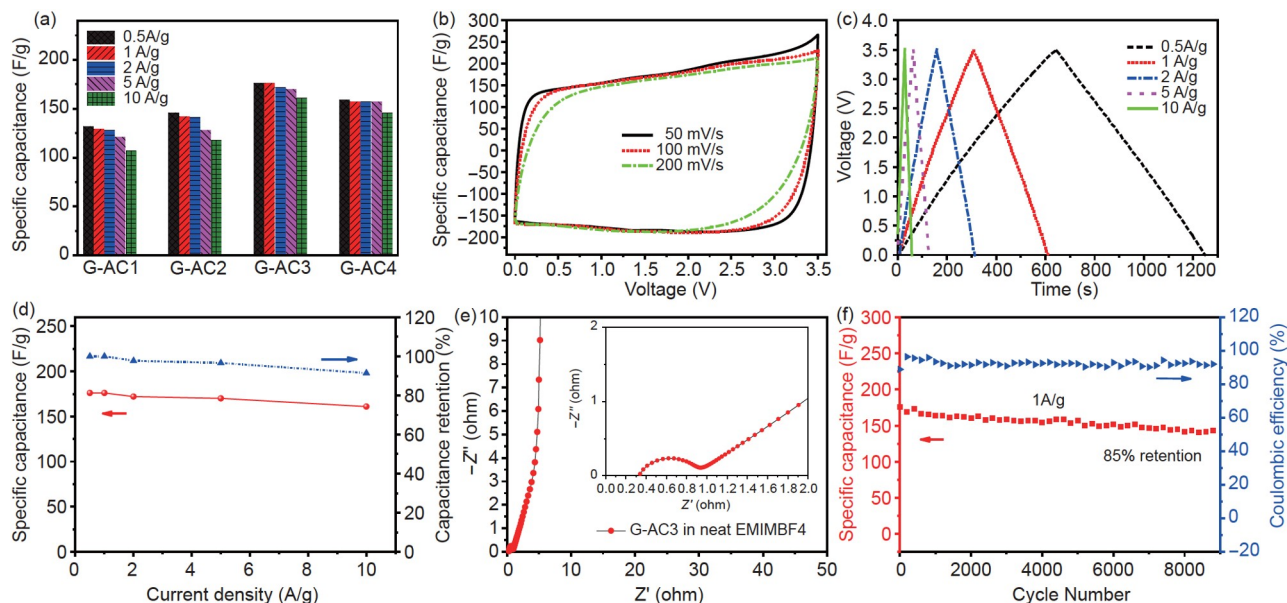


Figure 5 (Color online) Electrochemical characterization of the G-AC n samples in neat EMIMBF $_4$ electrolyte. (a) Specific capacitances of G-AC n at different current densities. (b) CV curves of G-AC3 at three different scan rates. (c) Galvanostatic charge/discharge curves of G-AC3 at different constant currents. (d) Rate performance of G-AC3. (e) Nyquist plots of the G-AC3-based supercapacitors. (f) Cycle life of G-AC3 at a current density of 1 A/g.

capacitances of optimized G-ACs (G-AC3) in 1 mol/L TEABF $_4$ /AN and neat EMIMBF $_4$ were 155 and 176 F/g at 1 A/g, respectively, thus having the high energy density, 39.2 and 74.9 W h/kg, respectively. In addition, the G-ACs exhibited excellent rate capability with negligible capacitance decay from 0.5 to 10 A/g in the 1 mol/L TEABF $_4$ /AN electrolyte and the neat EMIMBF $_4$ electrolyte. Furthermore, G-AC3 demonstrates an excellent energy density (68.5 W h/kg) and an ultra-high power density (8501 W/kg). Considering the low cost and abundance of asphalt resource, the scalability of the method, and the excellent electrochemical performance of devices fabricated using the synthesized G-ACs, these G-ACs are promising for developing cost-effective supercapacitors.

This work was supported by the National Natural Science Foundation of China (Grant No. 21905297), Guangdong Provincial Universities Characteristic Innovation Project (Grant No. 2019KTSCX120), Science and Technology Program of Guangzhou (Grant Nos. 202102010378, 202102020331), and Open Fund of the State Key Laboratory of Luminescent Materials and Devices, South China University of Technology (Grant No. 2019-skllmd-06).

Supporting Information

The supporting information is available online at tech.scichina.com and link.springer.com. The supporting materials are published as submitted, without typesetting or editing. The responsibility for scientific accuracy and content remains entirely with the authors.

- Zhang M, Xiang L, Galluzzi M, et al. Uniform distribution of alloying/dealloying stress for high structural stability of an Al anode in high-area-density lithium-ion batteries. *Adv Mater*, 2019, 31: 1900826
- Wang J W, Liu X H, Mao S X, et al. Microstructural evolution of tin

nanoparticles during *in situ* sodium insertion and extraction. *Nano Lett*, 2012, 12: 5897–5902

- Zhang G, Guan T, Wang N, et al. Small mesopore engineering of pitch-based porous carbons toward enhanced supercapacitor performance. *Chem Eng J*, 2020, 399: 125818
- Feng X, Shi X, Ning J, et al. Recent advances in micro-supercapacitors for ac line-filtering performance: From fundamental models to emerging applications. *eScience*, 2021, 1: 124–140
- Sim Y, Surendran S, Cha H, et al. Fluorine-doped graphene oxide prepared by direct plasma treatment for supercapacitor application. *Chem Eng J*, 2022, 428: 132086
- Su F, Wu Z S. A perspective on graphene for supercapacitors: Current status and future challenges. *J Energy Chem*, 2021, 53: 354–357
- Jung S H, Thi Huong P, Sahani S, et al. Biomass-derived graphene-based materials embedded with onion-like carbons for high power supercapacitors. *J Electrochem Soc*, 2022, 169: 010509
- Huang Y, Gao A, Song X, et al. Supramolecule-inspired fabrication of carbon nanoparticles *in situ* anchored graphene nanosheets material for high-performance supercapacitors. *ACS Appl Mater Interfaces*, 2016, 8: 26775–26782
- Yin X, Zhang J, Yang L, et al. Carbon electrodes with ionophobic characteristics in organic electrolyte for high-performance electric double-layer capacitors. *Sci China Mater*, 2022, 65: 383–390
- Mou X, Ma J, Zheng S, et al. A general synthetic strategy toward highly doped pyridinic nitrogen-rich carbons. *Adv Funct Mater*, 2021, 31: 2006076
- Qu Y, Lu C, Su Y, et al. Hierarchical-graphene-coupled polyaniline aerogels for electrochemical energy storage. *Carbon*, 2018, 127: 77–84
- Sui D, Xu L, Zhang H, et al. A 3D cross-linked graphene-based honeycomb carbon composite with excellent confinement effect of organic cathode material for lithium-ion batteries. *Carbon*, 2020, 157: 656–662
- Sui D, Chang M, Wang H, et al. A brief review of catalytic cathode materials for Na-CO $_2$ batteries. *Catalysts*, 2021, 11: 603
- Jeong J H, Lee G W, Kim Y H, et al. A holey graphene-based hybrid supercapacitor. *Chem Eng J*, 2019, 378: 122126
- Meng C, Das P, Shi X, et al. *In situ* and operando characterizations of 2D materials in electrochemical energy storage devices. *Small Sci*, 2021, 1: 2000076

- 16 Zheng S, Wu Z S, Wang S, et al. Graphene-based materials for high-voltage and high-energy asymmetric supercapacitors. *Energy Storage Mater*, 2017, 6: 70–97
- 17 Zhang L, Zhang F, Yang X, et al. Porous 3D graphene-based bulk materials with exceptional high surface area and excellent conductivity for supercapacitors. *Sci Rep*, 2013, 3: 1408
- 18 Lu Y, Long G, Zhang L, et al. What are the practical limits for the specific surface area and capacitance of bulk sp^2 carbon materials? *Sci China Chem*, 2016, 59: 225–230
- 19 Zhang M, Sun Z, Zhang T, et al. Porous asphalt/graphene composite for supercapacitors with high energy density at superior power density without added conducting materials. *J Mater Chem A*, 2017, 5: 21757–21764
- 20 Zhang R, Yan J, Wang L, et al. Achieving ion accessibility within graphene films by carbon nanofiber intercalation for high mass loading electrodes in supercapacitors. *J Power Sources*, 2021, 513: 230559
- 21 Yang Z, Tian J, Yin Z, et al. Carbon nanotube- and graphene-based nanomaterials and applications in high-voltage supercapacitor: A review. *Carbon*, 2019, 141: 467–480
- 22 Yang W, Deng B, Hou L, et al. N, S codoped hierarchical porous graphene nanosheets derived from petroleum asphalt via *in situ* texturing strategy for high-performance supercapacitors. *Ind Eng Chem Res*, 2019, 58: 4487–4494
- 23 Pan L, Li X, Wang Y, et al. 3D interconnected honeycomb-like and high rate performance porous carbons from petroleum asphalt for supercapacitors. *Appl Surf Sci*, 2018, 444: 739–746
- 24 He X, Zhang N, Shao X, et al. A layered-template-nanospace-confinement strategy for production of corrugated graphene nanosheets from petroleum pitch for supercapacitors. *Chem Eng J*, 2016, 297: 121–127
- 25 Cao S, Yang J, Li J, et al. Preparation of oxygen-rich hierarchical porous carbon for supercapacitors through the co-carbonization of pitch and biomass. *Diam Relat Mater*, 2019, 96: 118–125
- 26 Pan L, Wang Y, Hu H, et al. 3D self-assembly synthesis of hierarchical porous carbon from petroleum asphalt for supercapacitors. *Carbon*, 2018, 134: 345–353
- 27 Xu C, Ning G, Zhu X, et al. Synthesis of graphene from asphaltene molecules adsorbed on vermiculite layers. *Carbon*, 2013, 62: 213–221
- 28 Oyekunle L O. Certain relationships between chemical composition and properties of petroleum asphalts from different origin. *Oil Gas Sci Tech-Rev IFP*, 2006, 61: 433–441
- 29 Petersen J C, Plancher H. Model studies and interpretive review of the competitive adsorption and water displacement of petroleum asphalt chemical functionalities on mineral aggregate surfaces. *Pet Sci Tech*, 1998, 16: 89–131
- 30 Petersen J C. A dual, sequential mechanism for the oxidation of petroleum asphalts. *Pet Sci Tech*, 1998, 16: 1023–1059
- 31 Ma Y, Chang H, Zhang M, et al. Graphene-based materials for lithium-ion hybrid supercapacitors. *Adv Mater*, 2015, 27: 5296–5308
- 32 Ji B, Zhang F, Wu N, et al. A dual-carbon battery based on potassium-ion electrolyte. *Adv Energy Mater*, 2017, 7: 1700920
- 33 Zhao J, Fan H, Li G, et al. Enlarging ion-transfer micropore channels of hierarchical carbon nanocages for ultrahigh energy and power densities. *Sci China Mater*, 2021, 64: 2173–2181
- 34 Kang D, Liu Q, Gu J, et al. “Egg-box”-assisted fabrication of porous carbon with small mesopores for high-rate electric double layer capacitors. *ACS Nano*, 2015, 9: 11225–11233
- 35 Chang P, Matsumura K, Wang C, et al. Frame-filling structural nanoporous carbon from amphiphilic carbonaceous mixture comprising graphite oxide. *Carbon*, 2016, 108: 225–233
- 36 Zhang L, Zhang F, Yang X, et al. High-performance supercapacitor electrode materials prepared from various pollens. *Small*, 2013, 9: 1342–1347
- 37 Zhu C, Liu T, Qian F, et al. Supercapacitors based on three-dimensional hierarchical graphene aerogels with periodic macropores. *Nano Lett*, 2016, 16: 3448–3456